Chapter 1

From Cyclodextrins to Amylose: Structures and Lipophilicity Patterns

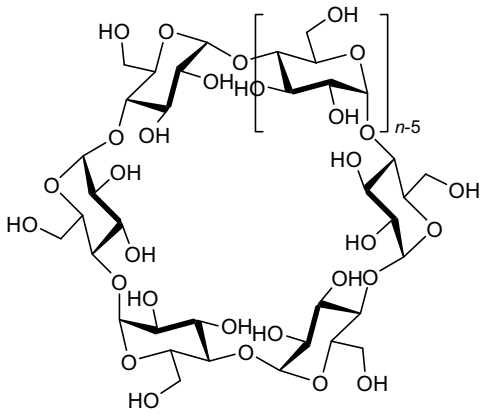

cyclodextrins

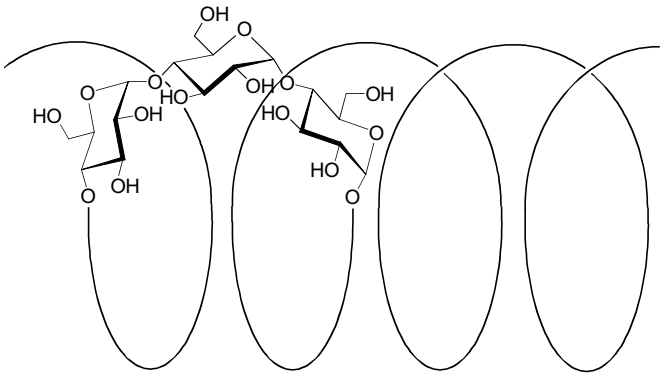

V_H-amylose

Topography of the 1:1 α-Cyclodextrin - Nitromethane Inclusion Complex

T. Nakagawa, S. Immel, F. W. Lichtenthaler, and H. J. Lindner,
Carbohydr. Res. **2000**, *324*, 141-146.

The Hydrophobic Topographies of Amylose and its Blue Iodine Complex

S. Immel and F. W. Lichtenthaler,
Starch/Stärke **2000**, *52*, 1-8.

ELSEVIER

www.elsevier.nl/locate/carres

Carbohydrate Research 324 (2000) 141–146

CARBOHYDRATE RESEARCH

Note

Topography of the 1:1 α-cyclodextrin–nitromethane inclusion complex☆

Toshio Nakagawa, Stefan Immel, Frieder W. Lichtenthaler *, Hans J. Lindner

Institut für Organische Chemie, Technische Universität Darmstadt, Petersenstraße 22, D-64287 Darmstadt, Germany

Received 23 August 1999; accepted 12 October 1999

Abstract

Dissolution of α-cyclodextrin (α-CD) in 9:1 water–nitromethane smoothly generates the title compound, which crystallizes as the pentahydrate in the orthorhombic space group $P2_12_12_1$ with $a = 9.452(4)$, $b = 14.299(3)$, $c = 37.380(10)$ Å, and $Z = 4$. Its crystal structure analysis revealed the α-CD macrocycle in an unstrained conformation stabilized through a ring of O-2···O-3′ hydrogen bonds between five of the six adjacent glucose residues. The nitromethane is located in the α-CD cavity in an orientation parallel to the plane of the macrocycle, and assumes two sites of equal population with the nitro group in excessive thermal motion; the guest is held by van der Waals contacts and C-H···O-type hydrogen bonds to the pyranose H-3 and H-5 protons. The packing of the macrocycles in the crystal lattice is of cage herringbone-type with an extensive intra- and intermolecular hydrogen bonding network. The ready formation of a nitromethane inclusion complex in aqueous nitromethane, and the subtleties of its molecular structure amply demonstrate the ease with which water is expelled from the α-CD cavity by a more hydrophobic co-solvent.

Keywords: α-Cyclodextrin; Nitromethane inclusion complex

1. Introduction

Various small organic molecules have been shown to be readily included into the apolar cavity of α-cyclodextrin (α-CD, Scheme 1), such as methanol [2], dimethylformamide [3], and dimethyl sulfoxide [4], and their topographies have been thoroughly characterized by solid-state structures. Surprisingly, nitromethane, a standard solvent as well as a reagent, has not been reported to complex with α-CD or any of the other cyclodextrins [5,6]. Here we report on the ready preparation of a 1:1 α-CD–CH_3NO_2 inclusion complex (**1**) and its topography on its X-ray based structure.

2. Results and discussion

The atomic numbering scheme and the molecular structure of the α-CD–nitromethane inclusion complex (**1**) are shown in Scheme 1 and Fig. 1; some averaged geometric parameters are listed in Table 1. The nitromethane is incorporated into the central cavity of the torus-shaped α-CD, and five

☆ Molecular modeling of saccharides, Part 23. For Part 22, see Ref. [1].

* Corresponding author. Tel.: +49-61-5116-2376; fax: +49-61-5116-6674.

E-mail address: fwlicht@sugar.oc.chemie.tu-darmstadt.de (F.W. Lichtenthaler)

water molecules occupy interstitial positions between the CD macrocycles in the crystal lattice. The CD macrocycles are arranged in a typical herringbone-type pattern in the crystal environment (space group $P2_12_12_1$, views along the *a* and *b* axis are given in Fig. 2), as is, for example, also found in the three α-CD hydrate solid-state structures [7–9].

Conformation of the macrocycle.—As indicated by the intersaccharidic Φ/Ψ torsion angles (cf. Table 1) and their rather small fluctuations, the α-CD macrocycle in **1** adopts its usual conical shape similar to the one realized in a large variety of related complexes [6,10,11]. The mean tilt angle τ [11,12] of the glucose units in relation to the macroring displays a slight rotation of the pyranoses with their 6-OH sides towards the center of the molecule (i.e., $\tau > 90°$), leaving the opposite 2-OH/3-OH face as the wider opening of the torus. All the 6-CH_2OH groups point away from the central axis of **1** (*gg* arrangements, $\omega \approx -70°$). The glucose units are in the rather rigid $^4C_1$ conformation with standard ring torsion angles $\Theta_1 - \Theta_6$ around $\pm 55°$, and with typical Cremer–Pople ring puckering parameters [13,14]. The intersaccharidic O-1 atoms are fairly coplanar (RMS deviation of only 0.06 Å from the common least-squares plane) and form a symmetrical hexagon with nearly identical diagonal distances of 8.45 ± 0.2 Å.

Hydrogen bonding.—The comparatively unrestrained overall geometry of the α-CD host is stabilized through an almost complete ring of O-2···O-3′ hydrogen bonds between five out of six adjacent glucose residues (cf. Fig. 3 and Table 2, hydrogen bonds labeled 1–5); and no other intramolecular hydrogen bonds are formed. However, the solid-state geometry displays an extensive three-dimensional hydrogen-bonding network between the α-CD, the five water molecules of crystallization (Table 2, entries 6–11), and the symmetry-related molecules in the crystal lattice (entries 12–30) as is usually observed for carbohydrate crystal structures [15]. All hydroxyl groups satisfy their hydrogen-bonding requirements through formation of two to three H-bonds, and all water molecules are involved in three to four H-bonds.

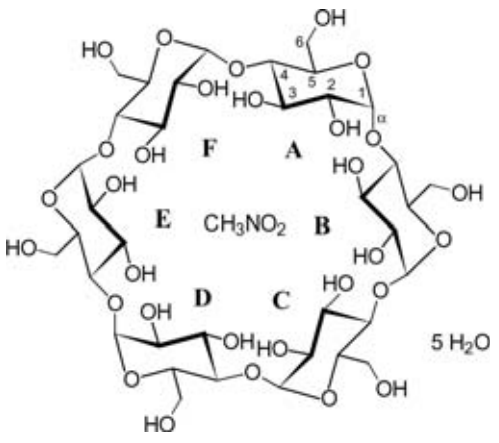

Scheme 1. α-Cyclodextrin–nitromethane inclusion complex (**1**); the α-(1→4)-linked glucose units are labeled A–F.

Geometry of the nitromethane inclusion.—The nitromethane molecule is located in the void of the α-CD macrocycle, with the methyl group being disordered over two sites with equal (50%) occupancy (Fig. 1), whereas the corresponding two nitrogen positions coincide in one fully occupied site. The oxygen atoms of the guest display excessive thermal motions (Fig. 1), indicating that the NO_2 group is statistically disordered; refinement of the structure was approximated by six positions over which the two oxygens are distributed (33% occupancy of each site). Only four 'reasonable' (in terms of bond angles) oxygen sites are retained in the ball-and-stick type representation of the complex, given in Fig. 4, with the superimposed molecular contact surfaces [16] visualizing the steric fit between the host and guest molecule. Side-view cross-sectional cuts through these surfaces (Fig. 4, bottom) show both nitromethane sites to be shifted away from the center of the α-CD torus towards the wider opening (i.e., the 2-OH/3-OH face). In either geometry, the nitromethane C–N bond points almost perpendicular away from the central axis of the complex. Obviously, the guest is held in the cavity by van der Waals contacts to a circular array of the pyranose hydrogens at C-3 and C-5. Although the NO_2 group is not involved in hydrogen bonds with the hydroxyl groups of the host, it does form hydrogen bonds of the O···H–C type to the C-3 and C-5 protons, respectively;

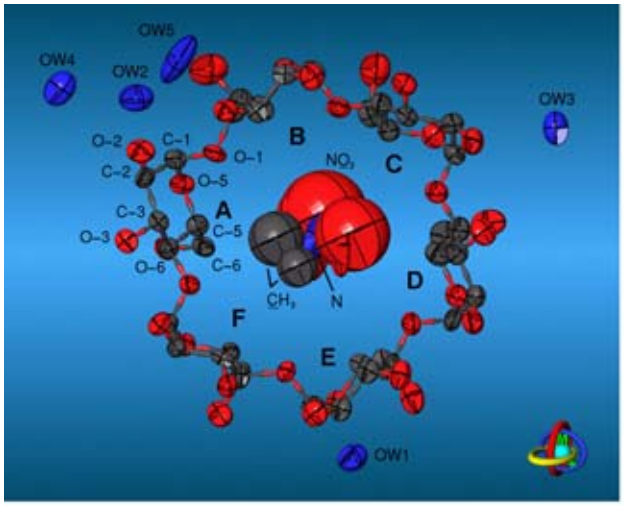

Fig. 1

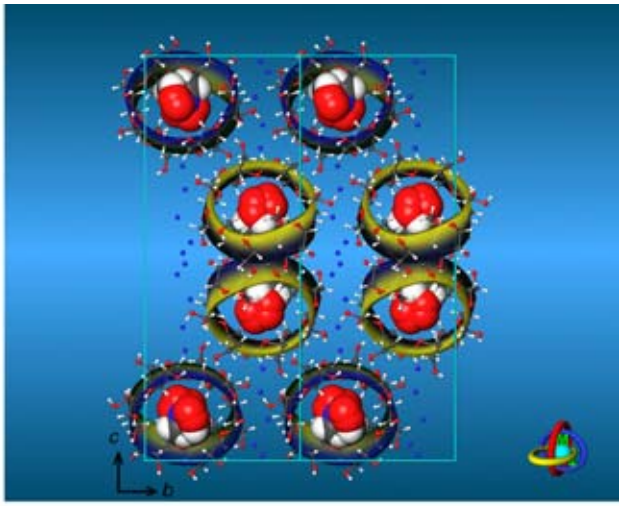

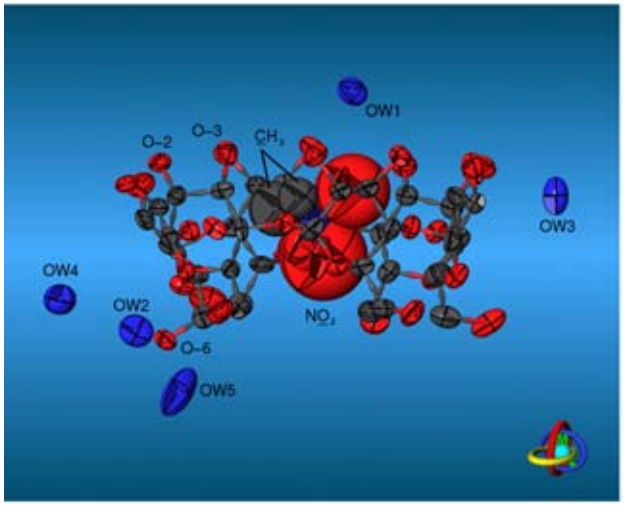

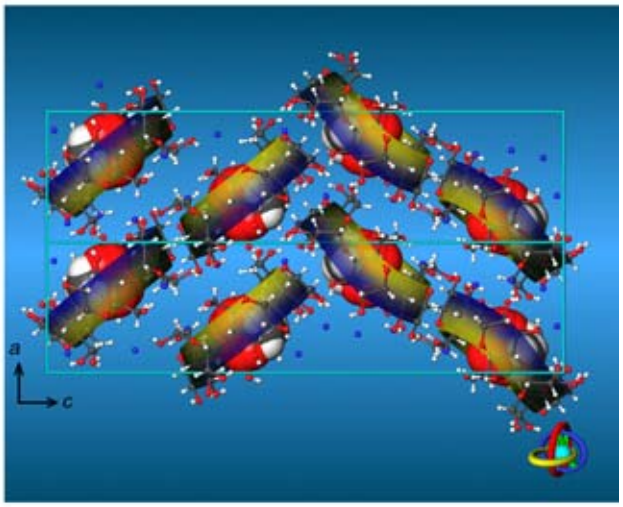

Fig. 2

Fig. 1. Molecular structure of the asymmetric unit of the α-CD–nitromethane inclusion complex (**1**) showing the heavy-atom 50% probability ellipsoids; hydrogens are omitted for clarity (gray, C; red, O; blue, nitrogen and water-oxygens). The glucose units of α-CD are labeled A–F (cf. Scheme 1), and the water molecules located at interstitial positions outside the macrocycle are termed OW1–OW5. The nitromethane guest molecule shows excessive thermal motions and is disordered over two sites with equal occupancies; the statistical disordering of the NO_2 oxygen atoms is approximated by six atomic positions.
Fig. 2. Ball-and-stick models of the herringbone-type molecular packing in the crystal structure of **1**, as viewed down the *a* (top, $1 \times 2 \times 1$ unit cells) and *b* axis (bottom, $2 \times 1 \times 1$ cells). The α-CD molecules are represented as solid colored ribbon models, whereby blue colors correspond to the 2-OH/3-OH side of the macrocycles, yellow colors to the 6-OH face. The disordered nitromethane molecules are visualized as CPK-models, and the unit cell boundaries are indicated by solid cyan lines.

for each NO_2-oxygen position the shortest O···H-3 and O···H-5 distances are in the range of 2.48–2.82 Å.

3. Conclusions

The solid-state structure of the α-CD–nitromethane pentahydrate complex shows that the mode with which the guest molecule is incorporated into the cavity results from a balance of at least two effects contributing to the stability of such assemblies; hydrophobic effects conceivably favor the hydrophobic methyl group pointing into the cavity, thereby leaving the nitro group to stick out of the α-CD torus at the opposite, hydrophilic rim, whereas the antiparallel arrangement of dipoles of host and guest would lead to the opposite regioselectivity. The inclusion of nitromethane almost perpendicular to the molecular axis displays a counterbalance of these effects, while the α-CD cavity itself is large enough to allow for excessive thermal

Table 1
Selected geometric parameters (mean values averaged over all glucose units and root mean-square deviations) for the α-CD macrocycle in **1**

Intersaccharidic torsion angles (°)	
Φ (O-5–C-1–O-1–C-4′)	107.4 ± 4.8
Ψ (C-l–O-1–C-4′–C-3′)	129.4 ± 11.3
Tilt angles	
τ (°)	101.6 ± 9.3
Pyranose torsion angles (°)	
ω (O-5–C-5–C-6–O-6)	−68.8 ± 7.3
Θ_1 (O-5–C-1–C-2–C-3)	57.6 ± 2.3
Θ_2 (C-l–C-2–C-3–C-4)	−51.8 ± 2.7
Θ_3 (C-2–C-3–C-4–C-5)	49.7 ± 3.4
Θ_4 (C-3–C-4–C-5–O-5)	−50.8 ± 3.3
Θ_5 (C-4–C-5–O-5–C-1)	58.2 ± 1.6
Θ_6 (C-5–O-5–C-1–C-2)	−62.0 ± 2.2
Cremer–Pople parameters	
Q (Å)	0.550 ± 0.023
θ (°)	5.5 ± 3.5
ϕ (°)	50.4 ± 29.7
Distances (Å)	
O-1(A)–O-1(D)	8.32
O-1(B)–O-1(E)	8.62
O-1(C)–O-1(F)	8.44

motions of the guest and rotation of the nitro group. The ready preparation of the complex, and the subtleties of its molecular structure presented here, amply demonstrate the ease with which water is expelled from the α-CD cavity by a co-solvent.

4. Experimental

Preparation of the α-cyclodextrin – nitromethane complex.—To a stirred solution of α-CD (2.49 g, 2.56 mmol) in water (25 mL) was added dropwise nitromethane (3 mL), and the reaction mixture was kept overnight in a refrigerator. The colorless crystals formed were collected by filtration and dried in a desiccator over silica gel: 1.79 g (62%). A second crop (0.70 g, 24%) was obtained from the mother liquor on evaporation to about one third of its volume, followed by saturation with nitromethane. The crystals became opaque at 90–100 °C and started browning at ~265 °C. $[\alpha]_D^{22}$ +130° (*c* 0.91, water); $[\alpha]_D^{22}$ +120° (*c* 0.90, water saturated with CH_3NO_2); IR (KBr): NO_2 asymmetric stretching vibration band at 1561 cm^{-1} and symmetric band at 1381 cm^{-1}; ^1H and ^{13}C NMR spectra of the complex in $[D_6]Me_2SO$ are of little significance, as they showed only minor chemical shift differences in comparison to those of pure α-CD as well as nitromethane in $[D_6]Me_2SO$, conceivably due to formation — in part at least — of an α-CD–$[D_6]Me_2SO$ complex by displacement of the nitromethane from the cavity. Anal. Calcd for $C_{36}H_{60}O_{30}\cdot CH_3NO_2\cdot 5\ H_2O$ (1123.96): C, 39.54; H, 6.55; N, 1.25. Found: C, 39.61; H, 6.41; N, 1.10.

The complex is stable at room temperature, yet loses nitromethane on heating to 110 °C in vacuum (90% after 12 h).

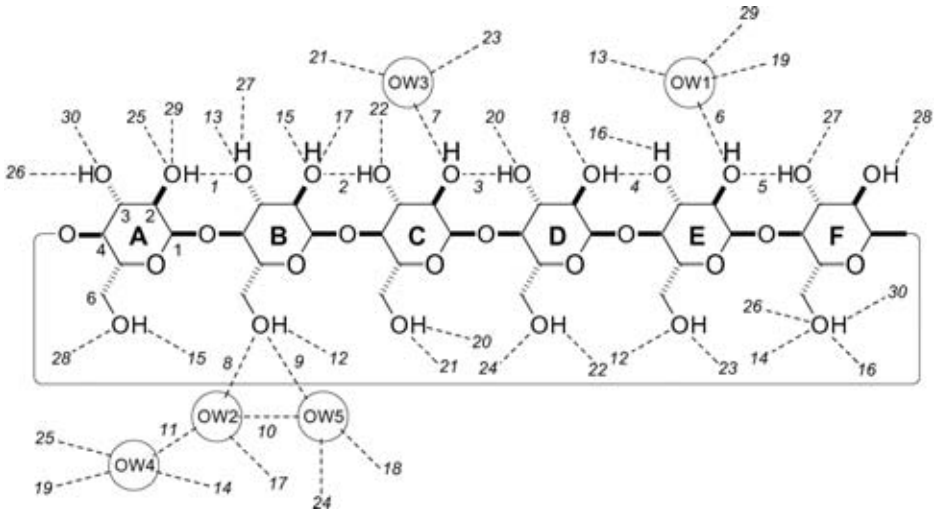

Fig. 3. Scheme of intra- and intermolecular hydrogen bonds in the solid-state structure of the α-CD–nitromethane pentahydrate inclusion complex (**1**). The individual glucose residues are labeled A–F and the water molecules OW1–OW5, the numbers in italics correspond to the indices given in Table 2; 'open-ended' lines indicate H-bonds formed between symmetry related positions. The nitromethane guest molecule is not involved in the hydrogen-bonding pattern.

Table 2
Hydrogen bonds in the solid-state structure of α-CD–nitromethane pentahydrate (**1**), listed for distances d(H···O) < 2.5 Å and/or d(O···O) < 3.2 Å only; the water molecules are labeled OW1–OW5, the glucose labeling A–F and the indices given in italics in the first column correspond to Fig. 3

No. (cf. Fig. 3)	Hydrogen bond	d(H···O) (Å) [a]	d(O···O) (Å)	ϕ(O–H···O) (°) [a]	Symmetry
1	O(2A)H···O(3B)	2.505	3.177	152.4	b
2	O(3C)H···O(2B)	2.295	3.030	172.5	b
3	O(3D)H···O(2C)	2.308	2.932	143.1	b
4	O(2D)H···O(3E)	2.192	2.899	159.9	b
5	O(3F)H···O(2E)	2.217	2.949	172.0	b
6	O(W1)···O(2E)		2.755		b
7	O(W3)···O(2C)		2.803		b
8	O(W2)···O(6B)		2.669		b
9	O(W5)···O(6B)		3.092		b
10	O(W5)···O(W2)		2.683		b
11	O(W4)···O(W2)		2.658		b
12	O(6B)H···O(6E)	2.136	2.864	168.8	c
13	O(3B)···O(W1)		2.834		c
14	O(W4)···O(6F)		2.978		c
15	O(6A)H···O(2B)	2.117	2.811	157.1	d
16	O(3E)H···O(6F)	2.056	2.788	172.1	e
17	O(2B)···O(W2)		2.628		e
18	O(2D)···O(W5)		2.657		f
19	O(W1)···O(W4)		3.008		f
20	O(6C)H···O(3D)	2.200	2.820	142.3	g
21	O(6C)···O(W3)		2.967		g
22	O(6D)H···O(3C)	2.341	2.927	137.4	h
23	O(6E)···O(W3)		2.780		h
24	O(6D)···O(W5)		2.646		i
25	O(2A)···O(W4)		2.852		j
26	O(3A)H···O(6F)	2.262	2.833	135.1	k
27	O(3B)H···O(3F)	2.366	2.817	120.9	k
28	O(2F)H···O(6A)	2.030	2.744	163.1	k
29	O(2A)···O(W1)		3.196		l
30	O(6F)H···O(3A)	2.200	2.833	144.3	l

[a] Hydrogen bond H···O distances and O–H···O angles omitted if hydrogen atoms were not located explicitly. Symmetry operations: [b] x, y, z. [c] $x, y+1, z$. [d] $x-1, y, z$. [e] $x+1, y, z$. [f] $x+1, y-1, z$. [g] $-x+1, y+1/2, -z+3/2$. [h] $-x+1, y-1/2, -z+3/2$. [i] $-x, y-1/2, -z+3/2$. [j] $x+1/2, -y+3/2, -z+2$. [k] $x+1/2, -y+1/2, -z+2$. [l] $x-1/2, -y+1/2, -z+2$.

Crystal structure determination.—Suitable crystals for solid-state structural analysis were obtained by slow crystallization from a 9:1 water–nitromethane solution. A colorless single crystal, of dimensions $0.25 \times 0.175 \times 0.15$ mm, was sealed in the presence of the mother liquor in a thin glass capillary, and then mounted on an Enraf–Nonius CAD-4 diffractometer with graphite-monochromated Mo K_α ($\lambda = 0.71093$ Å) radiation: prisms, orthorhombic, space group $P2_12_12_1$ with $a = 9.452(4)$, $b = 14.299(3)$, and $c = 37.380(10)$ Å, $V = 5052.1(27)$ Å^3, $Z = 4$, $T = 298(2)$ K, μ(Mo K_α) = 0.126 mm^{-1}, and $D_x = 1.465$ Mg m^{-3}. A total of 5158 reflections were collected of which 5004 were independent ($R_{int} = 0.1236$). The structure was solved by direct methods using SHELXS-86 [17] and successive Fourier difference synthesis. Refinement (on F^2) was performed by full-matrix least-squares method with SHELXL-93 [18]. $R(F) = 0.0812$ for 3270 reflections with $I \geq 2\sigma I$, $\omega R(F^2) = 0.2762$ for 5004 reflections with $\omega = 1/(\sigma^2(F_o^2) + (0.1747P)^2 + 12.1519P$; where $P = (F_o^2 + 2F_c^2)/3$. All non-hydrogen atoms were refined anisotropically. Hydrogen atoms were considered in calculated positions with the $1.2 \times U_{eq}$ value of the corresponding atom; hydroxyl protons on the cyclodextrin were treated as idealized OH groups. Data reduction was

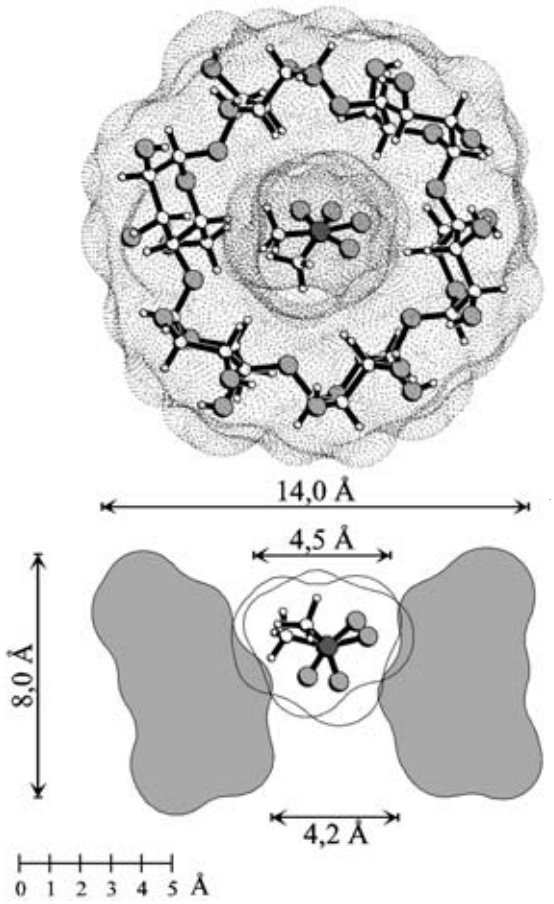

Fig. 4. Topology of the α-CD–nitromethane inclusion complex (**1**) with the water molecules located at the CD outside left off for clarity. Top: Contact surfaces in dotted form with a ball-and-stick model insert, viewed from the wider opening (2-OH/3-OH side) of the truncated cone; oxygen and nitrogen atoms are shaded. — Bottom: Side-view surface cross sections through the complex (2-OH/3-OH face at top); approximate molecular dimensions are given in Å.

done by a Stoe-REDU4 program, for atomic coordinates any further details see Section 5. The molecular graphics of Figs. 1, 2 and 4 were generated by the MolArch$^+$ program [19].

5. Supplementary material

Table of atomic coordinates, bond lengths and bond angles have been deposited with the Cambridge Crystallographic Data Centre as supplementary publication no. CCDC 136109. Copies of the data can be obtained free of charge on application to CCDC, 12 Union Road, Cambridge CB2 1EZ, UK (Fax: +44-1223-336033 or e-mail: deposit@ccdc.cam.ac.uk). Supporting information and additional molecular representations will be provided on the Internet in our graphics gallery at: http://caramel.oc.chemie.tu-darmstadt.de/immel/molcad/gallery.html.

Acknowledgements

The authors thank the Fonds der Chemischen Industrie, Frankfurt, for support of this work, Mrs Sabine Foro for collecting the crystallographic data, and Dr. T. Wimmer, Wacker-Chemie, Burghausen, for a generous gift of α-CD.

References

[1] H. Gohlke, S. Immel, F.W. Lichtenthaler, *Carbohydr. Res.*, 321 (1999) 96–104.
[2] B. Hingerty, W. Saenger, *J. Am. Chem. Soc.*, 98 (1976) 3357–3365.
[3] K. Harata, *Bull. Chem. Soc. Jpn.*, 52 (1979) 2451–2459.
[4] K. Harata, *Bull. Chem. Soc. Jpn.*, 51 (1978) 1644–1648.
[5] K. Harata, in J. Szejtli, T. Osa (Eds.), *Comprehensive Supramolecular Chemistry*, Vol. 3, Pergamon, Oxford, 1996, pp. 279–304.
[6] M.V. Rekharsky, Y. Inoue, *Chem. Rev.*, 98 (1998) 1875–1917 particularly Table 1.
[7] K.K. Chacko, W. Saenger, *J. Am. Chem. Soc.*, 103 (1981) 1708–1715.
[8] B. Klar, B. Hingerty, W. Saenger, *Acta Crystallogr., Sect. B*, 36 (1980) 1154–1165.
[9] K. Lindner, W. Saenger, *Acta Crystallogr., Sect. B*, 38 (1982) 203–210.
[10] K. Lipkowitz, *Chirality*, 4 (1992) 205–215.
[11] F.W. Lichtenthaler, S. Immel, *Liebigs Ann. Chem.*, (1996) 27–37.
[12] S. Immel, J. Brickmann, F.W. Lichtenthaler, *Liebigs Ann. Chem.*, (1995) 929–942.
[13] D. Cremer, J.A. Pople, *J. Am. Chem. Soc.*, 97 (1975) 1354–1358.
[14] G.A. Jeffrey, J.H. Yates, *Carbohydr. Res.*, 74 (1979) 319–322.
[15] G.A. Jeffrey, W. Saenger, *Hydrogen Bonding in Biological Structures*, Springer-Verlag, Berlin, 1991.
[16] M.L. Connolly, *J. Appl. Cryst.*, 16 (1983) 548–558. (b) M.L. Connolly, *Science*, 221, 709–713.
[17] G.M. Sheldrick, SHELXS-86, Program for the Solution of Crystal Structures, University of Göttingen, Germany, 1990.
[18] G.M. Sheldrick, SHELXL-93, Program for the Refinement of Crystal Structures, University of Göttingen, Germany, 1993.
[19] S. Immel, MolArch$^+$–MOLecular ARCHitecture Modeling Program, Darmstadt University of Technology, Germany, 1999.

The Hydrophobic Topographies of Amylose and its Blue Iodine Complex[1, 2]

Stefan Immel and Frieder W. Lichtenthaler,
Darmstadt (Germany)

Two polymorphs of amylose, the native double-helical A-form and the single-stranded V_H counterpart, as well as the amylose polyiodide complex were subjected to a molecular modeling study. Based on their X-ray diffraction-derived structures, the "solvent-accessible" contact surfaces were generated, onto which the computed molecular lipophilicity profiles (MLPs) were projected in color-coded form, easily allowing to locate hydrophobic and hydrophilic surface regions. Their detailed analysis revealed the double-stranded A-form to be a rather compact structure with an irregular distribution of hydrophilic and hydrophobic regions over the entire outer surface, with the interior of the double helix being inaccessible even for small molecules. By contrast, V_H-amylose, in accord with its water solubility, has a pronouncedly hydrophilic outside surface with an as distinctly hydrophobic channel. – In the dark-blue amylose-polyiodide complex, the hydrophobic channel of the single-helical V_H-form serves as a well-ordered matrix for incorporation and alignment of the iodine-iodide species to elaborate a linear polyiodide chain in a nearly perfect steric fit and in full complementarity of hydrophobic regions of guest and host. Thus, the MLPs provide substantive credence to the view, that not only the amylose-iodine complex formation is mediated to an essential degree by hydrophobic attractions at the guest-host interface, but that the same factors determine the stability of this unique supramolecular assembly.

Keywords: Amylose; Starch-iodide complex; α-Cyclodextrin-iodide, Inclusion compounds; Hydrophobicity patterns

1 Introduction

Amylose, the unbranched portion of starch, is the classical example of a linear polysaccharide composed of several thousand α(1→4)-linked D-glucose units, which adopts a helical structure. Fig. 1 provides a common textbook pictorial representation of this structure [3].

Besides leaving open whether the helix includes a central channel or not, this sketchy formulation of a single-stranded helix does not correctly depict the molecular organization of native amylose, since the two major amylose polymorphs A and B are double helical assemblies [4–7]. Single helixes of the type depicted above, with six glucose units per turn, are only obtainable in the form of inclusion complexes with dimethyl sulfoxide [8], *n*-butanol [9, 10], *n*-pentanol [10], or in a dry (V_A-amylose) or hydrated state (V_H-form) [11–13] upon removing the organic solvents entrapped in these complexes.

As the solid-state structures may be considered as "frozen" molecular images of their solution conformations – a presupposition that has yielded in the case of cyclodextrins [14] and their inclusion complexes [15] – we have entered the V_H- [13] and A-type amylose [4, 5] as well as the amylose-iodine complex [16, 17] into a detailed molecular modeling study, comprising generation of their molecular geometries, their contact surfaces, and – most relevant in terms of understanding their inclusion capabilities – their lipophilicity patterns. The results [2] are subject of this paper.

2 Experimental

2.1 Molecular structures

The molecular models of the A- and V_H-form of amylose were generated from atomic coordinates obtained from X-ray fiber diffraction [5, 13]. For A-amylose, two strands of 12 glucose units each were generated (two turns of the double helix, ≡ 2 · $C_{72}H_{122}O_{61}$), for V_H-amylose and the amy-

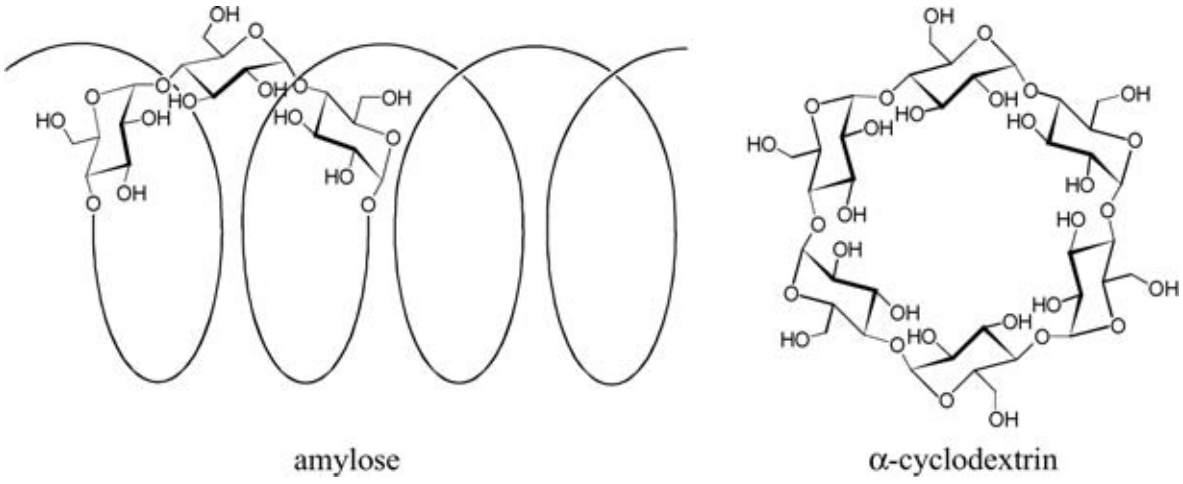

Fig. 1. Sketch representation of a left-handed, single-stranded helix of V_H-amylose (*left*), adapted from [3], where incorrectly a right-handed helix is depicted, and of α-cyclodextrin (*right*), which de facto represents a single turn of the amylose helix excised and re-connected by *Bacillus macerans*-derived enzymes (CGTases). The close analogy allows to consider V_H-amylose as a tubular analog of the cyclodextrins.

lose-iodine complex five single-stranded turns of altogether 30 glucose residues were used (≡ $C_{180}H_{302}O_{151}$) resulting in molecular dimensions of approximately 12 × 12 × 45 Å each. The solid-state structure of the *bis*-α-cyclodextrin/lithium triiodide-iodine octahydrate inclusion complex [29], i.e. $[C_{36}H_{60}O_{30}]_2 \cdot LiI_3 \cdot I_2 \cdot 8\ H_2O$ was obtained from the CCDF-Cambridge Crystallographic Data File (Refcode: CYDXLI10). Hydrogen atoms not included in the molecular structure determinations were positioned geometrically with standard bond lengths $r_{C–H}$ = 1.08 Å and $r_{O–H}$ = 0.90 Å, taking intramolecular hydrogen bonding interactions between spatially neighboring hydroxyl groups into account. All molecular parameters discussed within this study (cf. Tab. 1) were re-calculated from these data sets.

2.2 Molecular surfaces and molecular lipophilicity patterns (MLPs)

Calculation of the molecular contact surfaces [19] and the corresponding MLPs was carried out by using the MOLCAD [18, 24, 25] molecular modeling program, whereby the MLPs were computed after removal of all iodine species and for each molecule separately. Surfaces for the inclusion complexes were generated for the guest and host molecules separately, and were subsequently reassembled to the complex; surfaces of the amylose models were generated only for the center sections of approx. 30 Å length each in order to exclude "end"-effects for the polysaccharides. Cyclodextrin cross-cut plots through the center of geometry were computed from the intersection of a plane with the molecular surfaces [19]; molecular plots were generated using the MolArch+ program [49]. Visualization of the MLP surface qualities was done by color-coded projection of the computed values onto these surfaces by applying texture mapping [25], the surfaces of the iodine species were colored according to the atomic types (pink), and no surfaces qualities are mapped. Scaling of the molecular hydrophobicity patterns was performed in relative terms for each molecule separately, and no absolute values are displayed.

3 Results and Discussion

3.1 Molecular geometries and hydrogen bonding patterns of A- and V_H-type amylose

The molecular models of A- [5] and V_H-amylose [13] were generated from their respective X-ray fiber diffraction data, using five single helix turns (= 30 glucose units) for V_H-amylose, and two turns of the double helix for its A-form (= two strands of 12 glucose units each). The resulting structures, each of approximately 12 × 12 × 45 Å in size, are shown in Fig. 2 in ball-and-stick type representation, with their molecular contact surfaces [18, 19] – closely resembling the solvent (water) accessible surfaces [20] – molded around the rear half, clearly revealing the distinct differences of the two assemblies: a well-elaborated central channel in the single-stranded V_H-amylose, obviously capable of accommodating guests of appropriate dimensions, versus the double-helical A-form with its two strands so narrowly intertwined as to leave no interstitial space [21]. This basic dissimilarity of the two forms is even more lucidly illustrated in the projections along the helix axis (Fig. 3): V_H-amylose has an overall helix diameter of approximately 13.5 Å, a channel of ≈ 5.4 Å width, and an axial pitch of ≈ 8.1 Å per turn, whilst the double-helical A-form reveals a substantial increase of the axial pitch (to 21.4 Å per double turn), requiring the helix

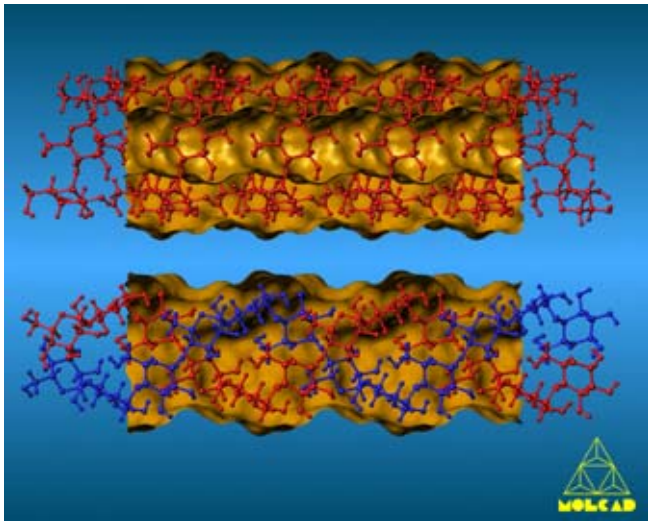

Fig. 2. Molecular geometries of V_H-type amylose (upper structure) and A-amylose (lower entry) [21]. Both forms consist of rod-shaped, left-handed helices of α(1→4)-linked glucose units with a uniform gauche-gauche arrangement of all hydroxymethyl groups in relation to their pyranoid rings. As V_H-amylose (*top*) represents a single helix of 6_5-symmetry, i.e. six glucose residues per left-handed turn, the model comprises five such turns, corresponding to a molecular composition of $C_{180}H_{302}O_{151}$ (axial spacing ≈ 8.05 Å per turn). The two individual strands of the double-helical A-form (*bottom*) of 2_1 symmetry (≡ 2 · $C_{72}H_{122}O_{61}$, two turns with a pitch of ≈ 21.4 Å per turn and 12 glucose units each) are colored blue and red, respectively, to facilitate identification. To exclude "end"-effects for the finite polymer segments of approximately 45 Å length each, the yellow-colored and half-opened contact surfaces (roughly equivalent to the solvent-accessible surfaces [19, 20], i.e. how closely water molecules can approach) are shown only for the center sections of ≈ 30 Å length.

diameter to decrease to 10.3 Å, thereby eliminating any central channel. Thus, it is easily understood, that the water of crystallization in the solid-state A-form is only located on places outside the helices.

Apart from strong van der Waals attractive forces that must be an important factor for establishing the distinctly different folding patterns – for the two intertwined single strands of the A-form in particular – the elaboration of a specific hydrogen bonding network undoubtedly is another. A computational assessment of the possible hydrogen bonding contacts between the two strands in A-amylose and between adjacent coils in the single-stranded V_H-form gave the following picture: the A-form of amylose establishes various hydrogen bond-mediated 2-O ⋯ O-6 contacts between glucose units of different strands (Fig. 4, left) with O ⋯ H distances of 1.9–2.1 Å and O–H ⋯ O angles in the range of 140–160° (Tab. 1, entries A–D). In V_H-amylose, however, not only 2-O ⋯ O-6 hydrogen bonds between spatially close glucose residues of the next spiral turn (Fig. 4, right entry and Tab. 1) are materialized, but these are also cooperatively strengthened by 2-O ⋯ O-3' hydrogen bonds between adjacent glucose units. The latter hydrogen bonds are – in agreement with *Jeffrey*'s and *Saenger*'s systematic analysis of H-bonding patterns in the crystal structures of carbohydrates [22] energetically highly favorable [23] and, by consequence, must be considered as an important factor in stabilizing the helical structures in amylose.

3.2 MLP profiles of A- and V_H-amylose

Since the formation of inclusion complexes of V-amylose is closely related to hydrophobic interactions within the

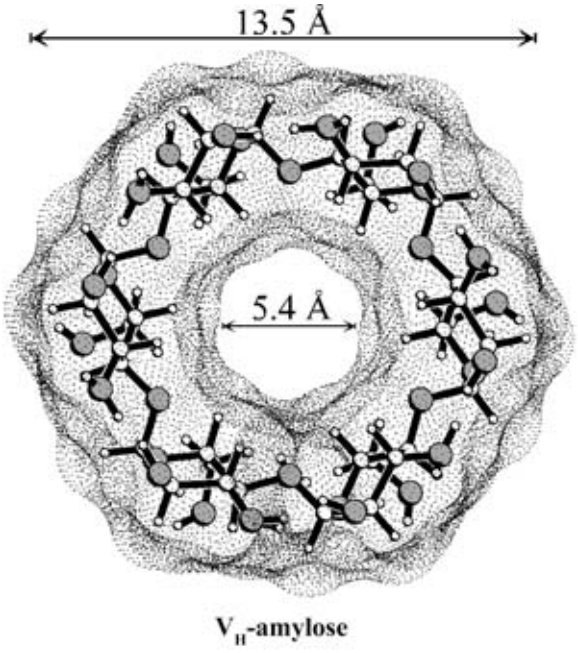

Fig. 3. Molecular surfaces (view along the helix axis) of V_H-amylose (*top*) and A-amylose (*bottom*), illustrating the molecular geometries of Fig. 2 and their approximate molecular dimensions.

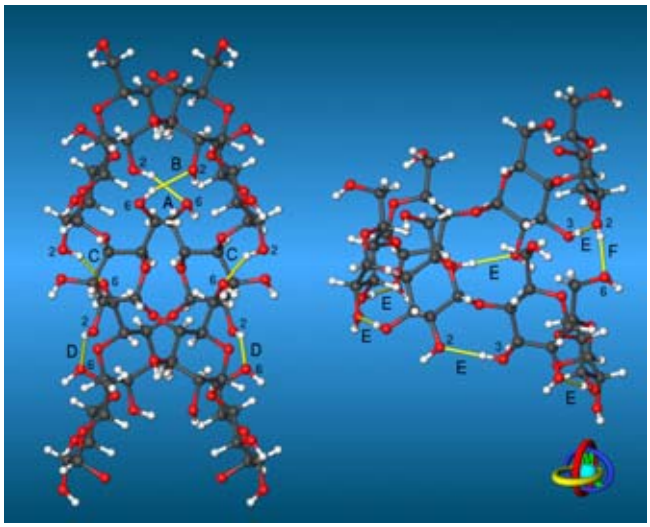

Fig. 4. Hydrogen bonding patterns (yellow lines) within the double helices of A-type starch (*left*) and the single helical V_H-type amylose (*right*), calculated from the heavy atom positions of the crystal structures. The letters refer to different types of hydrogen bonds, of which the geometry parameters are listed in Tab. 1.

channel, it was deemed important to get an anticipation of the distribution of hydrophobic and hydrophilic regions on the surfaces of the A- and V_H-polymorphs by generation of the respective molecular lipophilicity patterns (MLPs). These MLPs [24] were calculated and mapped onto the corresponding molecular contact surfaces of Fig. 2 by using the MOLCAD-program [18], and were visualized [24, 25] by applying a color-code graded into 32 shades, ranging from dark blue for the most hydrophilic surface regions to full yellow for the most hydrophobic areas.

As is apparent from the color-coded representations in Fig. 5 – the half opened surface models in the lower picture are particularly lucid in this respect – the hydrophobic characteristics of the V_H-amylose and the A-form differ significantly. The latter exhibits an irregular distribution of hydrophobic and hydrophilic outer surface areas (Fig. 5, lower models each), as contrasted by the pronouncedly hydrophilic (blue) outside surface regions of V_H-amylose (Fig. 5, top models): the outside surface regions are intensely hydrophilic (blue) – in accord with its comparatively high solubility in water – while its center channel is decisively hydrophobic (yellow). This distinctive inside-outside separation of hydrophobic and hydrophilic domains obviously preconditions the incorporation of iodide/iodine into the chan-

Tab. 1. Calculated hydrogen bond geometries (distances and angles) for the A- and V_H-form of amylose. The letters denote the different types of H-bonds as marked in Fig. 4.

Compound	Type of hydrogen bond (cf. Fig. 4)		Distances [Å]		Angle [°]
			d (O ··· H)	*d* (O ··· O)	φ (O-H ··· O)
A-amylose	**A**	2-OH ··· O-6[a]	2.08	2.93	158
	B	6-OH ··· O-2[a]	2.08	2.93	157
	C	2-OH ··· O-6[a]	1.90	2.75	156
	D	2-OH ··· O-6[a]	1.91	2.65	139
V_H-amylose	**E**	3-OH ··· O-2[b]	1.94	2.84	177
	F	2-OH ··· O-6[c]	1.95	2.78	154

[a] Interstrand hydrogen bonds.
[b] H-bond between adjacent glucose units.
[c] H-bond between glucose units in adjacent turns.

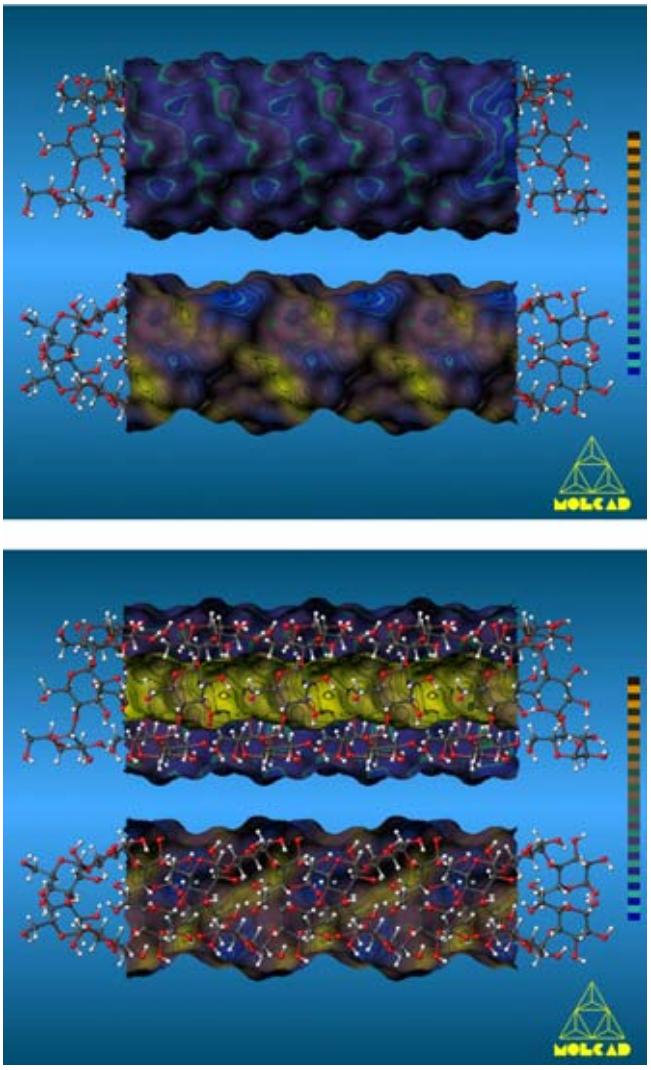

Fig. 5. Hydrophobic topographies for the amylose fraction of starch [21]: the MLP pattern (blue: hydrophilic surface regions, yellow: hydrophobic areas) on the contact surface of single-stranded V_H-amylose (upper structures each) is set against the parallel-stranded double-helical A-form (lower model, respectively). In both cases, fragments of approximately 45 Å length are shown, with the surfaces being depicted for the center sections of the rod-shaped polymers only (≈ 30 Å, cf. Fig. 2). The outside surface area of V_H-type amylose is uniformly hydrophilic (in conformity with its solubility in water) whereas the center channel is as distinctly hydrophobic-predestined to incorporate equally hydrophobic guests such as iodine or fatty acids. By contrast, the double-helical A-form of amylose, devoid of a center channel, exhibits an irregular distribution of hydrophilic and hydrophobic regions over the entire surface [26].

nel as a successive linear chain of I_2/I_3^- molecules [16], or of fatty acids [27] and a variety of other guests [8–10].

3.3 α-Cyclodextrin-iodine inclusions: models for the blue amylose-iodine complex?

As α-cyclodextrin represents an enzymatically excised and then re-connected single turn of the V_H-amylose helix (cf. Fig. 1) and, hence, may be considered a projection down its helix axis, its capability to form inclusion complexes with iodine [28] and polyiodide [29–31] may parallel that of amylose and serve as a conjectural model for the well-known deep-blue stained amylose-iodine-iodide complex. Accordingly, the generation of the molecular lipophilicity profiles and an assessment of the complementarity of the hydrophobic domains of guest (iodine) and host (α-CD) were considered relevant in this context.

Co-crystallization of α-CD with various polyiodides yields dark-brown to dark-blue stained complexes, which exhibit entirely different, infinite channel-type solid-state structures with approximately linear alignments of the polyiodide ions along the central axis [28–32]. Most notably, the *bis*-α-cyclodextrin lithium pentaiodide octahydrate complex $(\alpha\text{-CD})_2 \cdot LiI_3 \cdot I_2 \cdot 8\ H_2O$ [29] comprises two crystallographically independent cyclodextrin units which are "fused together" to a head-to-head dimer through an intense hydrogen bonding network between the secondary hydroxyl groups of the two α-CD tori (Fig. 6). Into the resulting "double cavity" formed by this assembly, the iodine atoms (four ordered positions and one disordered) are embedded with unequal iodine-iodine distances (mean value ≈ 3.1 Å). The Li^+ counter-ion is located outside this dimer assembly, hence out of range of strong electrostatic interactions with the anion [29].

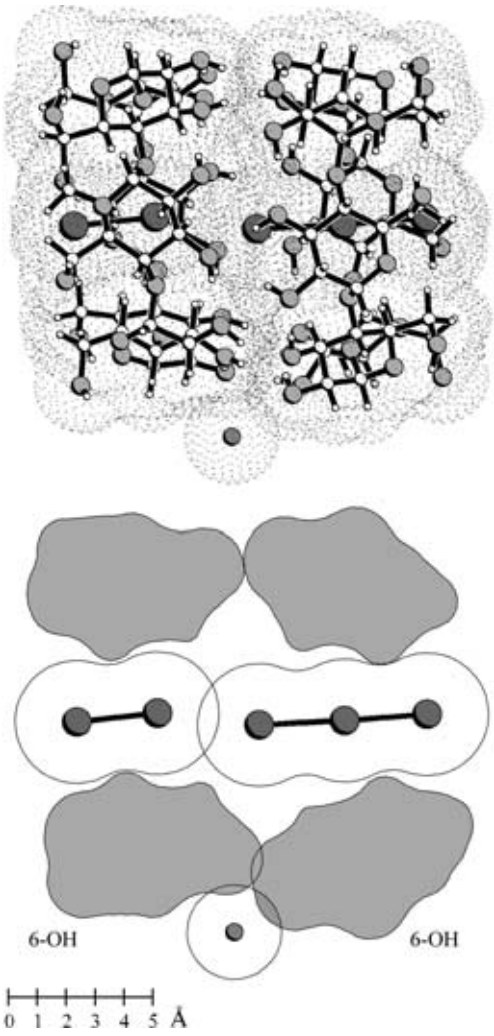

Fig. 6. *Top:* Ball-and-stick model and contact surface (in dotted form) of the complex $(\alpha\text{-CD})_2 \cdot LiI_3 \cdot I_2 \cdot 8\ H_2O$, as it emerged from its X-ray structure [29], with the water of crystallization removed for clarity. The basic unit of this assembly consists of two α-CD's forming a head-to-head-dimer through an intense hydrogen bonding network between the secondary 2- and 3-OH groups at their wider torus rims; the resulting "double cavity" is filled with an almost linear iodine-triiodide chain (represented by black balls in the center) with the counter-ion Li^+ (small sphere) located at the interstice. *Bottom:* Surface cross-section cut through the center of the dimer assembly exposing the five iodine atoms included.

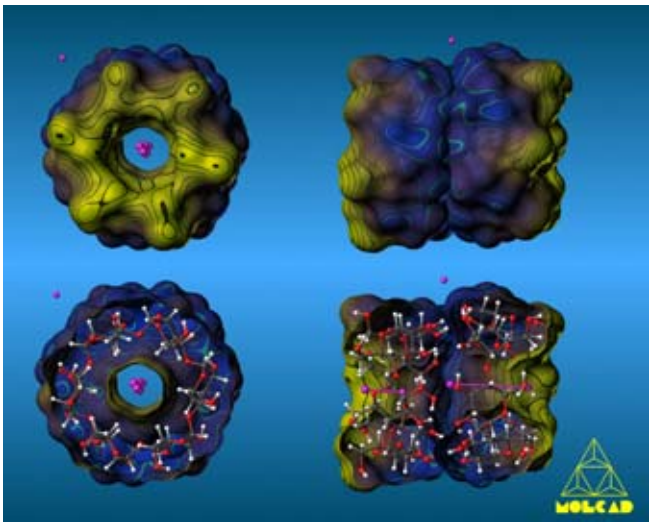

Fig. 7. Molecular lipophilicity patterns (MLPs) for the (α-CD) · LiI_3 · I_2 · 8 H_2O complex [29] of which the water of crystallization has been removed for clarity [21]. *Left:* View along the central channel axis, perpendicular to the α-CD mean planes. *Right:* Side-view models representing the hydrophobic topographies of the dimeric units. The location of the lithium ion is indicated by the isolated pink ball at the lower, half-opened models.

Generation of the MLPs of this complex and their color-coded projection onto the contact surfaces given in Fig. 6 provides the picture in Fig. 7, illustrating the assembly of the two α-CD macrocycles via their pronouncedly hydrophilic (blue) 2-OH/3-OH-sides which entails the two end sites, carrying the primary hydroxyl groups, to be as distinctly hydrophobic (yellow). Accordingly, the pentaiodide chain is packed into a channel-like "double cavity" with successive, alternating hydrophobic and hydrophilic surface regions.

Thus, the *bis*-α-CD – pentaiodide unit, due to its "finite" dimeric nature, provides only a limited analogy to the polymeric "infinite" amylose-iodine complex. However, when taking into account the packing of these dimeric units in the crystal lattice, a surprisingly close similarity emerges: infinite stacks with the elaboration of a somewhat uneven nanotube into which a nearly linear, continuous polyiodide chain is embedded as exemplified in Fig. 8. That this is materialized despite the alternating hydrophobic and hydrophilic zones along these nanotube channels is a strong indication for the pronounced proclivity of iodine or polyiodide species to associate with suitable hosts to polymeric supramolecular assemblies.

3.4 The amylose-iodine complex

The presence of iodine as well as iodide in aqueous solutions of amylose is a mandatory prerequisite for the formation of the blue complex [17], and binding occurs in a cooperative way by slow formation of stable I_{11}^{3-} nuclei inside the helices and rapid linear propagation [33]. With increasing iodide concentration the bluing species (polymeric unit of approx. $(C_6H_{10}O_5)_{16.5} \cdot I_6$ [34]) seems to change from I_{10}^{2-} to I_8^{2-} and I_6^{2-} [35], simultaneously shifting the maximum absorption towards shorter wavelengths. The enthalpy of the amylose-iodine interaction is rather large with –50 to –90 kJ per mole molecular iodine bound [36]. All of these data give evidence that the solid-state structure of the amylose-iodine complex [16] (Fig. 9) is a useful model even for the solution

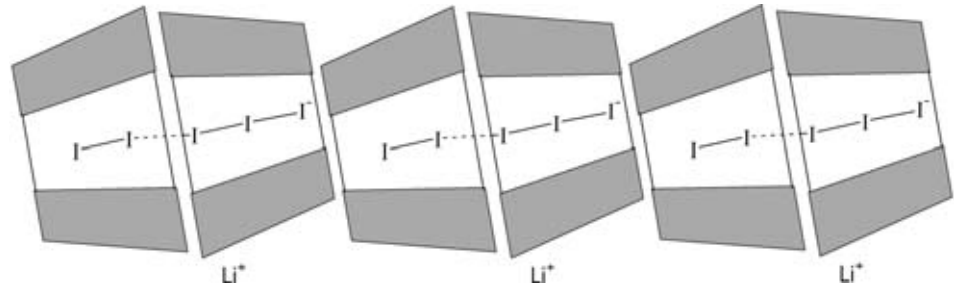

Fig. 8. Simplified illustration of the nearly nanotube-like stacking of the $(\alpha\text{-CD})_2$-pentaiodide units in the crystal lattice, thereby forming a continuous linear poly-iodine/iodide chain, an "endless" channel so to say.

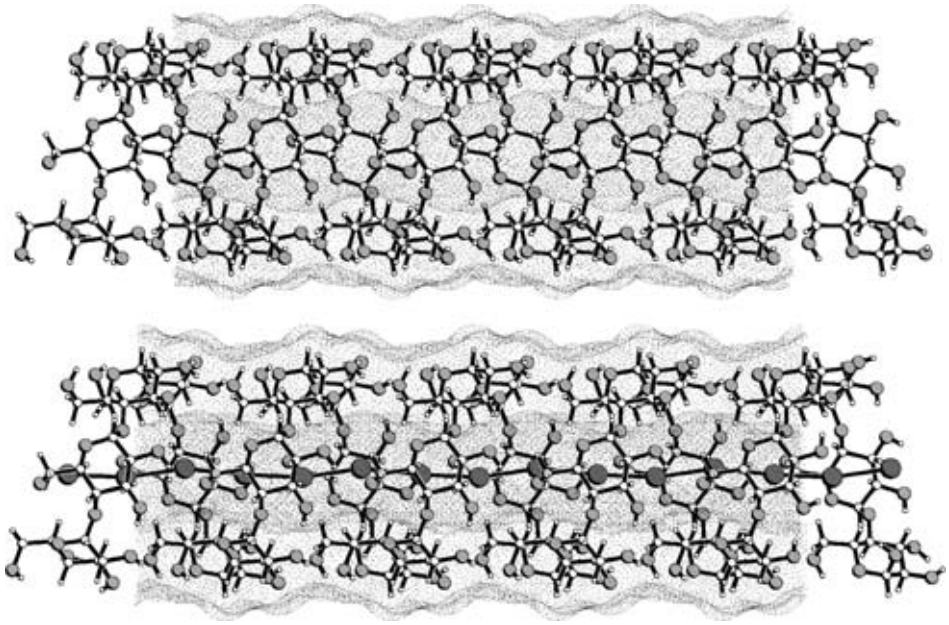

Fig. 9. Molecular geometry of the V_H-amylose with an "empty" channel (*top,* representation corresponding to Fig. 5) and with the essentially linear polyiodide chain (filled balls in the center) embedded (*bottom*), based on X-ray diffraction data [16] and calculation of the "solvent-accessible" contact surfaces [21].

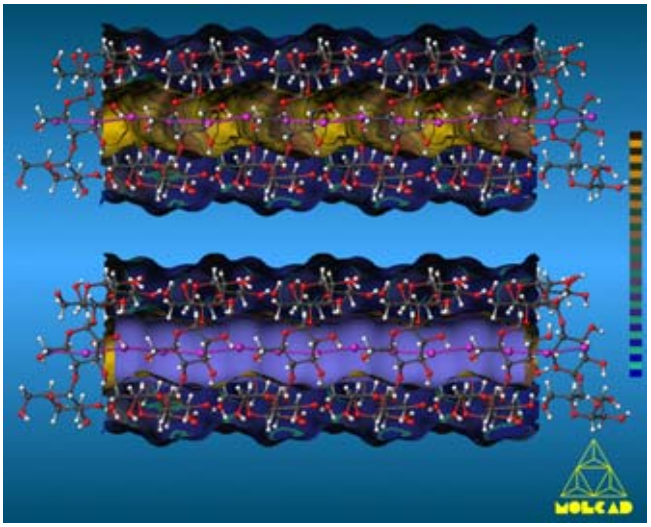

Fig. 10. Molecular lipophilicity profile (MLP) for the V_H-amylose-iodine-iodide complex [21]. *Top:* half-opened model based on its solid-state structure [16] with the linear polyiodide chain (pink balls) in the channel; the hydrophobicity distribution is essentially identical to that of the non-complexed V_H-structure (Fig. 5). *Bottom:* The linear polyiodide chain inserted into the central channel with its half-opened contact surface (violet area behind the pink balls) to illustrate the perfect steric fit.

state: a nearly linear polyiodide chain with I ··· I-separations of ≈ 2.91, 2.91 and 2.99 Å, respectively, with the fiber repeat of the amylose helix (≈ 8.17 Å) slightly increased over that of iodine-free V_H-amylose (≈ 8.05 Å).

Generation of the contact surfaces of V_H-amylose and its polyiodine/iodide complex as depicted in Fig. 9, and the corresponding color-coded representation of the MLP profiles in Fig. 10, impressively illustrates the pronouncedly hydrophobic central channel which serves as a matrix for incorporation and alignment of the iodine species. Superimposition of the amylose helix with the iodine chain and its (pink-colored) contact surface (bottom structure of Fig. 10) documents the sterically perfect correspondence. The ideal guest-host complementarity not only manifests itself in a perfect fit of an almost linear iodine/iodide chain in an equally linear channel – not infinite in length, but long enough to include several consecutive polyiodide units but also in the matching of their hydrophobic domains.

Thus, the MLP profiles provide substantive credence to the view that amylose-iodine complex formation – to a very substantial degree – is mediated by the operation of attractive hydrophobic forces at the guest-host interface and provides a major element for engendering the stability of this unique supramolecular assembly.

4 Conclusion

The hydrophobic nature of the tubular channel in V_H-amylose and of the conical cavity in the cyclodextrins has been postulated and de facto taken for granted ever since their molecular structural features began to unravel about 60 years ago [37–39]. Yet still today, the "hydrophobic effect" – even if one has agreed on the exact definition of the term [40] – is an "elusive" entity; it can neither be quantified reliably, nor can it be separated from the various other factors involved in inclusion complex formation, such as guest-host correspondence of steric features, minimization of dipole-dipole interactions, and compensation of entropic and enthalpic parameters associated with changes in solvation.

The computation and visualization of hydrophobic and hydrophilic surface regions described here for amylose and its iodine inclusion complex not only permits – for the first time – a genuine and reproducible localization and differentiation of these regions. As significant is that the importance of complementary hydrophilic and hydrophobic surface domains at the guest-host interface is imposingly verified, their interplay thus being a decisive element in incorporation of the guest into the host.

Finally, the insights provided by these novel views at amylose – substantiated by similar results described elsewhere on the cyclodextrins [14, 15, 41], cyclomannins [41], cyclorhamnins [42], cycloaltrins [43–45], cyclogalactins [41, 46], cyclofructins [47], and on sucrose [48] – may not only provide a viable base for the preparation of new, useful inclusion complexes of amylose, but also for the design of new ensuing reactions towards a targeted exploitation of the chemistry of starch.

Acknowledgements

The authors are grateful to Prof. *J. Brickmann,* Institut für Physikalische Chemie, Technische Universität Darmstadt, for generously providing us access to his MOLCAD modeling software package [18].

Bibliography

[1] This account is Part 24 of the series "Molecular Modeling of Saccharides". Part 23: *T. Nakagawa, S. Immel,* and *F. W. Lichtenthaler*: Topography of a 1:1 α-cyclodextrin – nitromethane inclusion complex. Carbohydr. Res. **324** (2000), 141–146.

[2] Portions of this work have been used by F.W.L. in his SPRI Science Award Lecture (Helsinki, 1995), of which an account has appeared: *F. W. Lichtenthaler* and *S. Immel:* Computersimulation of chemical and biological properties of sucrose, the cyclodextrins, and amylose. Internat. Sugar J. **97** (1995), 12–22.

[3] *P. M. Collins* and *R. J. Ferrier:* Monosaccharides, their chemistry and their roles in natural products. Wiley, Chichester/New York 1995, p. 490.

[4] *H.-C. H. Wu* and *A. Sarko:* The double-helical molecular structure of crystalline A-amylose. Carbohydr. Res. **61** (1978), 27–40.

[5] *A. Imberty, H. Chanzy, S. Pérez, A. Buléon,* and *V. Tran:* The double-helical nature of the crystalline part of A-starch. J. Mol. Biol. **201** (1988), 365–378.

[6] *H.-C. H. Wu* and *A. Sarko:* The double-helical molecular structure of crystalline B-amylose. Carbohydr. Res. **61** (1978), 7–25.

[7] *A. Imberty* and *S. Pérez:* A revisit to the three-dimensional structure of B-type starch. Biopolymers **27** (1988), 1205–1221.

[8] [8a] *A. French* and *H. F. Zobel:* X-Ray diffraction of oriented amylose fibers. The amylose-dimethyl sulfoxide complex. Biopolymers **5** (1967), 457–464.
[8b] *W. T. Winter* and *A. Sarko:* Crystal and molecular structure of the amylose-DMSO complex Biopolymers **11** (1972), 849–852; **13** (1974), 1461–1468.

[9] *R. E. Rundle* and *F. C. Edwards:* The configuration of the starch-iodine complex. An X-ray diffraction investigation of butanol-precipitated amylose. J. Am. Chem. Soc. **65** (1943), 2200–2203.

[10] *W. Hellert* and *H. Chanzy:* Single crystals of V amylose complexed with *n*-butanol or *n*-pentanol: structural features and properties. Int. J. Biol. Macromol. **16** (1994), 207–213.

[11] *B. Zaslow, V. G. Murphy,* and *A. D. French:* V-amylose-water system. Structural changes resulting from hydration. Biopolymers **13** (1974), 779–790.

[12] *P. Zugenmaier* and *A. Sarko:* Packing analysis of carbohydrates and polysaccharides. B-Amylose. Biopolymers **15** (1976), 2121–2136.

[13] *G. Rappenecker* and *P. Zugenmaier:* Detailed Refinement of the crystal structure of V_H-amylose. Carbohydr. Res. **89** (1981), 11–19.

[14] *S. Immel* and *F. W. Lichtenthaler:* On the hydrophobic characteristics of cyclodextrins: computer-aided visualization of molecular lipophilicity patterns. Liebigs Ann. Chem. (1996), 27–37.

[15] *F. W. Lichtenthaler* and *S. Immel:* Towards understanding formation and stability of cyclodextrin-inclusion complexes: computation and visualization of their lipophilicity patterns. Starch/Stärke **48** (1996), 145–154.

[16] *T. L. Bluhm* and *P. Zugenmaier:* Detailed structure of the V_H-amylose-iodine complex: A linear polyiodide chain. Carbohydr. Res. **89** (1981), 1–10.

[17] *K. A. Murdoch:* The amylose-iodine complex. Carbohydr. Res. **233** (1992), 161–174.

[18] [18a] *J. Brickmann:* MOLCAD – MOLecular Computer Aided Design, Technische Hochschule Darmstadt, 1996. The major part of the MOLCAD-program is included in the SYBYL package of TRIPOS Associates, St. Louis, USA.
[18b] *J. Brickmann:* Molecular graphics – how to see a molecular scenario with the eyes of a molecule. J. Chim. Phys. **89** (1992), 1709–1721.
[18c] *J. Brickmann, T. Goetze, W. Heiden, G. Moeckel, S. Reiling, H. Vollhardt,* and *C.-D. Zachmann:* Interactive visualization of molecular scenarios with MOLCAD/SYBYL. In: Data Visualization in Molecular Science – Tools for Insight and Innovation (Ed.: J. E. Bowie), Addison-Wesley Publ., Reading, Mass. 1995, pp. 83–97.

[19] *M. L. Connolly:* Solvent-accessible surfaces of proteins and nucleic acids. Science **221** (1983), 709–713.

[20] *B. Leek* and *F. M. Richards:* Interpretation of protein structures: estimation of static accessibility. J. Mol. Biol. **55** (1971), 379–400.

[21] All 3D-structures can be viewed on the WWW at: http://caramel.oc.chemie.tu-darmstadt.de/immel/3Dstructures.html; MOLCAD graphies are available at: http://caramel.oc.chemie.tu-darmstadt.de/immel/molcad/gallery.html.

[22] *G. A. Jeffrey* and *W. Saenger:* Hydrogen bonding in biological structures. Springer Verlag, Berlin/New York 1991, chapter 13, pp. 169–219.

[23] *I. Tvaroska* and *S. Pérez:* Conformational-energy calculations for oligosaccharides: a comparison of methods. Carbohydr. Res. **149** (1986), 389–410.

[24] *W. Heiden, G. Moeckel,* and *J. Brickmann:* A new approach to analysis and display of local lipophilicity/hydrophilicity mapped on molecular surfaces (MLP). J. Comput.-Aided Mol. Des. **7** (1993), 503–514.

[25] *M. Teschner, C. Henn, H. Vollhardt, S. Reiling,* and *J. Brickmann:* Texture mapping, a new tool for molecular graphics. J. Mol. Graphics **12** (1994), 98–105.

[26] The V_H-amylose part of this figure, first published in a lecture account [2], has been used as the frontispiece of a book: Carbohydrates as Organic Raw Materials III. Eds. *H. van Bekkum, H. Röper,* and *A. G. J. Voragen:* VCH Publ., Weinheim/New York 1996.

[27] [27a] *T. L. G. Carlson, K. Larsson, N. Dinhguyen,* and *N. Krog:* A study of the amylose-monoglyceride complex by Raman spectroscopy. Starch/Stärke **31** (1979), 222–224.
[27b] *R. Stute* and *G. Konieczny-Janda:* DSC studies on starch-lipid complexes. Starch/Stärke **35** (1983), 340–347.
[27c] *S. Raphaelides* and *J. Karkalas:* Thermal dissociation of amylose-fatty acid complexes. Carbohydr. Res. **172** (1988), 65–82.
[27d] *G. Wulff* and *S. Kubik:* Helical amylose complexes with organic ligands. Macromol. Chem. **193** (1992), 1071–1080.
[27e] *G. Wulff* and *S. Kubik:* Circular dichroism and UV spectroscopy of complexes of amylose. Carbohydr. Res. **237** (1992), 1–10.
[27f] *S. Kubik* and *G. Wulff:* Characterization and chemical modification of amylose complexes. Starch/Stärke **45** (1993), 220–225.

[28] *R. K. McMullan, W. Saenger, J. Fayos,* and *D. Mootz:* Topography of cyclodextrin inclusion complexes. Molecular geometry of the iodine-cyclohexaamylose complex. Carbohydr. Res. **31** (1973), 211–227.

[29] *M. Noltemeyer* and *W. Saenger:* Structural chemistry of linear α-cyclodextrin-polyiodide complexes. Models for the blue amylose-iodine complex. J. Am. Chem. Soc. **102** (1980), 2710–2722.

[30] *F. Cramer, U. Bergmann, P. C. Manor, M. Noltemeyer,* and *W. Saenger:* Lineare Polyiodidketten in kanalförmiger Cyclodextrin-matrix. Kristallographische Daten und Vergleiche mit dem blauen Stärke-Polyiodid-Komplex. Liebigs Ann. Chem. (1976), 1169–1179.

[31] *C. Betzel, B. Hingerty, M. Noltemeyer, G. Weber, W. Saenger,* and *J. A. Hamilton:* β-Cyclodextrin compound with potassium iodide. Spatial fitting of a polyiodide chain to a given matrix. J. Inclusion Phenom. Mol. Recogn. **1** (1983), 181–191.

[32] *W. J. James, D. French,* and *R. E. Rundle:* Schardinger dextrins. Structure of the cyclohexaamylose-iodine complex. Acta Crystallogr. Sect. B **12** (1959), 385–389.

[33] [33a] *J. C. Thompson* and *E. Hamori:* A kinetic investigation of the amylose-iodine reaction. J. Phys. Chem. **75** (1972), 272–280.
[33b] *A. Cesàro, J. C. Benegas,* and *D. R. Ripoll:* Molecular model of the cooperative amylose-triiodide complex. Phys. Chem. **90** (1986), 2787–2791.

[34] *M. Minick, K. Fotta,* and *A. Khan:* Polyiodine units in starch-iodine complex; INDO CI study of spectra. Biopolymers **31** (1991), 57–63.

[35] [35a] *G. A. Gilbert* and *J. V. R. Marriot:* Starch-iodine complexes. Trans. Faraday Soc. **44** (1948), 84–93.
[35b] *T. Handa, H. Yajima,* and *T. Kajiura:* On the blue color of triiodide ions in starch and starch fractions. Raman spectra of bluing species in amylose. Biopolymers **19** (1980), 1723–1741.

[36] [36a] *W. Banks, C. T. Greenwood,* and *K. M. Khan:* The interaction of linear amylose oligomers with iodine. Carbohydr. Res. **17** (1971), 25–33.
[36b] *A. Cesàro, E. Jerian,* and *S. Saule:* Physicochemical studies of amylose in aqueous solution: thermodynamics of the iodine-triiodide complex. Biopolymers **19** (1980), 1491–1506.
[36c] *T. Handa, H. Yajima, T. Yamamura, T. Ishii,* and *H. Aikawa:* Enthalpy change of amylose triiodide formation. Starch/Stärke **32** (1980), 194–197.

[37] [37a] *K. Freudenberg, E. Schaaf, G. Dumpert,* and *Th. Ploetz:* Neue Ansichten über die Stärke. Naturwiss. **27** (1939), 850–853.
[37b] *K. Freudenberg* and *H. Boppel:* Die Lage der Verzweigungsstelle in der Stärke. Ber. Dtsch. Chem. Ges. **73** (1940), 609–620.

[38] [38a] *D. French* and *R. E. Rundle:* The molecular weights of the Schardinger α- and β-dextrins. J. Am. Chem. Soc. **64** (1942), 1651–1653.
[38b] *R. E. Rundle:* The configuration of starch in the starch-iodine complex. Fourier-projections from X-ray diagrams. J. Am. Chem. Soc. **69** (1947), 1769–1772.

[39] *R. H. Marchessault* and *A. Sarko:* X-ray structure of polysaccharides. Adv. Carbohydr. Chem. **22** (1967), 421–481, particularly p. 468 ff.

[40] *W. Blokzijl* and *J. B. F. N. Engeberts:* Hydrophobic effects, opinion and facts. Angew. Chem. **105** (1993), 1610–1624; Angew. Chem. Int. Ed. Engl. **32** (1993), 1545–1559.

[41] *F. W. Lichtenthaler* and *S. Immel:* Cyclodextrins, cyclomannins, and cyclogalactins with five and six (1→4)-linked sugar units: a comparative assessment of their conformations and hydrophobicity potential profiles. Tetrahedron Asymmetry **5** (1994), 2045–2060.

[42] *F. W. Lichtenthaler* and *S. Immel:* The lipophilicity patterns of cyclodextrins and non-glucose cyclooligosaccharides. J. Inclusion Phenom. Mol. Recogn. Chem. **25** (1996), 3–16.

[43] *Y. Nogami, K. Nasu, T. Koga, K. Ohta, K. Fujita, S. Immel, H. J. Lindner, G. E. Schmitt,* and *F. W. Lichtenthaler:* Synthesis, structure and conformational features of α-cycloaltrin: a cyclooligosaccharide with alternating $^4C_1/^1C_4$ pyranoid chairs. Angew. Chem. **109** (1997), 1987–1991; Angew. Chem. Int. Ed. Engl. **36** (1997), 1899–1902.

[44] *S. Immel, K. Fujita,* and *F. W. Lichtenthaler:* Solution geometries and lipophilicity patterns of α-cycloaltrin. Chem. Eur. J. **5** (1999), 3185–3192.

[45] *K. Fujita, W. H. Chen, D.-Q. Yuan, Y. Nogami, T. Koga, T. Fujioka, M. Mihyshi, S. Immel,* and *F. W. Lichtenthaler:* Guest-induced conformational change in a flexible host: mono-*altro*-β-cyclodextrin. Tetrahedron Asymmetry **10** (1999), 1689–1696.

[46] *H. Gohlke, S. Immel,* and *F. W. Lichtenthaler:* Conformations and lipophilicity profiles of some cyclic β(1 → 3)- and β(1 → 6)-linked oligogalactofuranosides. Carbohydr. Res. **321** (1999), 96–104.
[47] *S. Immel, G. E. Schmitt,* and *F. W. Lichtenthaler:* Cyclofructins with six to ten β(1 → 2)-linked fructofuranose units: geometries, lipophilicity patterns, and potential for inclusion complexation. Carbohydr. Res. **313** (1998), 91–105.
[48] *F. W. Lichtenthaler* and *S. Immel:* Sucrose, sucralose, and fructose: Correlations between hydrophobicity potential profiles and AH-B-X assignments, in: Sweet Taste Chemoreception. Eds. *M. Mathiouthi, J. A. Kanters,* and *G. G. Birch.* Elsevier Applied Science, London/New York 1993, pp. 21–53.
[49] *S. Immel:* MolArch+-MOLecular ARCHitecture Modeling Program, Technische Universität Darmstadt, 1999.

Address of authors: Professor Dr. Dr.h.c. *Frieder W. Lichtenthaler* and Dr. *Stefan Immel.* Institut für Organische Chemie, Technische Universität Darmstadt. Petersenstraße 22, D-64287 Darmstadt (Germany).

(Received: August 23, 1999).

  0038-9056/2000/0101-0008$17.50+.50/0